

Studies of Quantum-Mechanical Coherency Effects in Neutrino-Nucleus Elastic Scattering

V. Sharma,^{1,2} L. Singh,^{1,3} H.T. Wong,^{1,*} M. Agartioğlu,^{1,4,5} J.-W. Chen,⁶ M. Deniz,⁴
S. Kerman,^{4,†} H.B. Li,¹ C.-P. Liu,⁵ K. Saraswat,¹ M.K. Singh,^{1,2} and V. Singh^{2,3}

(TEXONO Collaboration)

¹ *Institute of Physics, Academia Sinica, Taipei 11529, Taiwan.*

² *Department of Physics, Institute of Science, Banaras Hindu University, Varanasi 221005, India.*

³ *Department of Physics, School of Physical and Chemical Sciences, Central University of South Bihar, Gaya 824236, India*

⁴ *Department of Physics, Dokuz Eylül University, Buca, İzmir 35160, Turkey.*

⁵ *Department of Physics, National Dong Hwa University, Shoufeng, Hualien 97401, Taiwan.*

⁶ *Department of Physics, CTS and LeCosPA, National Taiwan University, Taipei 10617, Taiwan.*

(Dated: May 11, 2021)

Neutrino-nucleus elastic scattering (νA_{el}) provides a unique laboratory to study the quantum-mechanical (QM) coherency effects in electroweak interactions. The deviations of the cross-sections from those of completely coherent systems can be quantitatively characterized through a coherency parameter $\alpha(q^2)$. The relations between α and the underlying nuclear physics in terms of nuclear form factors are derived. The dependence of cross-section on $\alpha(q^2)$ for the various neutrino sources is presented. The $\alpha(q^2)$ -values are evaluated from the measured data of the COHERENT CsI and Ar experiments. Complete coherency and decoherency conditions are excluded by the CsI data with $p=0.004$ at $q^2=3.1\times 10^3$ MeV² and with $p=0.016$ at $q^2=2.3\times 10^3$ MeV², respectively, verifying that both QM superpositions and nuclear many-body effects contribute to νA_{el} interactions.

PACS numbers: 13.15.+g, 03.65.-w, 21.10.Ft

Keywords: Neutrino Interactions, Quantum Mechanics, Nuclear Form Factors

I. INTRODUCTION

The elastic scattering of a neutrino with a nucleus [1, 2]

$$\nu A_{el}: \quad \nu + A(Z, N) \rightarrow \nu + A(Z, N) \quad , \quad (1)$$

where $A(Z, N)$ denotes the atomic nucleus with its respective atomic, charge and neutron numbers, is a fundamental electroweak neutral current process in the Standard Model (SM).

Studies of neutrino-nucleus elastic scattering can provide sensitive probes to physics beyond SM (BSM) [3, 4] and certain astrophysical processes [1, 5]. It offers prospects to study quantum-mechanical (QM) coherency effects in electroweak interactions [6], neutron density distributions [7], to detect supernova neutrinos [8] and to provide a compact and transportable neutrino detectors for real-time monitoring of nuclear reactors [9]. The νA_{el} events from solar and atmospheric neutrinos are the irreducible “neutrino floor” background [10] to the coming generations of dark matter experiments [11].

There are several active experimental programs to observe and measure the νA_{el} processes with neutrinos from reactors [12] or from decay-at-rest pions (DAR- π) [4] provided by spallation neutron source [13]. Future dark matter experiments may also be sensitive to νA_{el} from solar neutrinos [14]. First positive measurement of νA_{el} was

achieved by the COHERENT experiment with CsI(Na) detector [15], followed by measurements with liquid Ar detector [16].

The νA_{el} interaction provides a laboratory to probe the QM coherency effects [6]. Experimental measurements are mostly performed in a parameter space where the coherency effects are partial and incomplete. The deviations from perfect coherency would have to be described and quantified before this interaction can be effectively applied towards other goals like the studies of BSM physics.

Coherency in QM superpositions among scattering amplitudes from individual nucleons is central to νA_{el} interactions. Our earlier work [6] identified a coherency parameter $\alpha(q^2)$ which can quantify and consistently characterize the degree of coherency in νA_{el} with different ν -sources and target nuclei. This article follows and expands on these studies. The relations between $\alpha(q^2)$ with the complementary descriptions in terms of nuclear physics via the language of nuclear form factors or with the reduction in cross-sections are discussed in Section II. The dependence of coherency effects with interaction kinematics for various neutrino sources and detector targets are surveyed in Section III. The constraints provided by the COHERENT-CsI and -Ar data are derived in Section IV.

*Corresponding Author: htwong@phys.sinica.edu.tw

†Deceased

II. FORMULATION AND CHARACTERIZATION

The νA_{el} differential cross-section at three-momentum transfer q ($\equiv |\vec{q}|$) and neutrino energy E_ν can be expressed as [2, 6]:

$$\left[\frac{d\sigma}{dq^2}(q^2, E_\nu) \right]_{\nu A_{el}} = \frac{1}{2} \left[\frac{G_F^2}{4\pi} \right] \cdot \left[1 - \frac{q^2}{4E_\nu^2} \right] \cdot \Gamma(q^2), \quad (2)$$

where $\Gamma(q^2)$ is a function describing the contributions due to many-body physics in the target nuclei, since the νA_{el} interactions involve collective contributions of individual nucleons in the nucleus.

The relevant kinematics variable is q^2 which characterizes the physics and is universal to all target. The experimental observable is the nuclear recoil energy (T), expressed in units of keV_{nr} in this article, which depends on the target nuclear mass M and is related to q^2 via $q^2=2MT+T^2 \simeq 2MT$. The minimal observable energy T_{min} for the nuclear recoils is the detector threshold, while kinematics limits the maximum recoil energy to be $T_{max}=2E_\nu^2/(M+2E_\nu) \simeq 2E_\nu^2/M$. These limits can be translated to $q_{min}^2=2MT_{min}$ and $q_{max}^2=4E_\nu^2[M/(M+2E_\nu)] \simeq 4E_\nu^2$. The variations of the νA_{el} differential and integral cross-sections with respect to T are discussed in Appendix A.

Depending on the particular physics aspects to probe, there are complementary formulations on the $\Gamma(q^2)$ function. The conventional description is based on nuclear physics, expressed as

$$\Gamma(q^2) \equiv \Gamma_{NP}(q^2) = [\varepsilon Z F_Z(q^2) - N F_N(q^2)]^2, \quad (3)$$

where $F_Z(q^2) \in [0, 1]$ and $F_N(q^2) \in [0, 1]$ are, respectively, the proton and neutron nuclear form factors for the nucleus $A(Z, N)$, while $\varepsilon \equiv (1 - 4 \sin^2 \theta_W) = 0.045$, indicating the dominant contributions are from the neutrons.

The merit of this description is to connect νA_{el} to nuclear physics so that its studies may benefit from or contribute to the wealth of information and data. Electron-nucleus scattering experiments provide important data to the nuclear proton form factor $F_Z(q^2)$ [17]. The neutron counterpart $F_N(q^2)$, however, would require weak processes to probe. Studies of νA_{el} have therefore triggered intense activities towards their measurements [7], complementing experiments with parity-violation scattering using polarized electrons [18].

In the kinematics regime relevant to this work – $q^2 R^2 \ll \pi^2$ (natural units with $\hbar=c=1$ are used throughout), where $R=1.2A^{1/3}$ fm is the typical scale characterizing the radius of nuclei – nucleons can be taken as structureless point-like particles, such that their internal dynamics and QCD effects can be neglected. At $q^2 \rightarrow 0$, there is a perfect alignment of the scattering amplitude vectors of individual nucleons in the target nucleus [6]. The interactions are completely coherent. As q^2 increases, deviation from this complete coherency

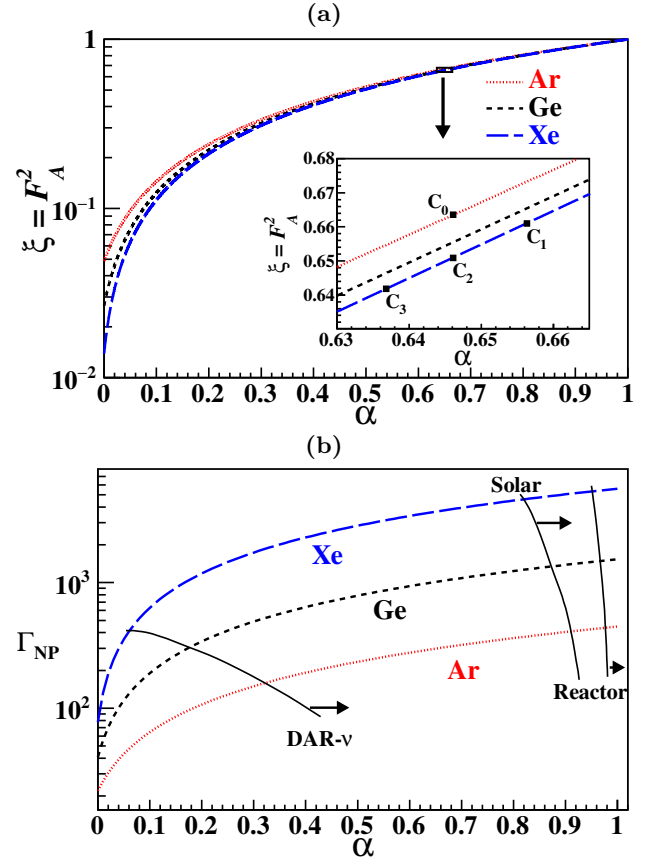


FIG. 1: The variations with α for (a) cross-section reduction fraction ξ (equivalently F_A) and (b) Γ_{NP} for the three target nuclei, independent of underlying nuclear physics. Superimposed in (b) are contours of maximum- q^2 for reactor, solar and DAR- π neutrinos. The limiting values are $\xi=1$ and $\Gamma_{NP}=(\varepsilon Z - N)^2$ at $\alpha=1$ and $\xi=(\varepsilon^2 Z + N)/(\varepsilon Z - N)^2$ and $\Gamma_{NP}=(\varepsilon^2 Z + N)$ at $\alpha=0$. The configurations $C_{0,1,2,3}$ in the inset of (a) illustrate the cases where $\alpha_0 < \alpha_1$, $\alpha_0 = \alpha_2$ and $\alpha_0 > \alpha_3$ despite having $F_A^2 = \xi$ and $\xi_0 > \xi_{1,2,3}$ in all cases.

condition leads to reduction in the cross-section. The degree of coherency can be quantified by a parameter $\alpha(q^2) \equiv \cos \phi \in [0, 1]$ where $\phi(q^2) \in [0, \pi/2]$ is the misalignment phase angle between the scattering amplitudes of two non-identical nucleons [6]. This leads to a formulation in terms of QM superpositions among the various scattering centers, in which:

$$\begin{aligned} \Gamma(q^2) &\equiv \Gamma_{QM}(q^2) \\ &= Z\varepsilon^2 [1 + \alpha(Z-1)] + N [1 + \alpha(N-1)] - 2\alpha\varepsilon ZN \\ &= (\varepsilon Z - N)^2 \cdot \alpha(q^2) + (\varepsilon^2 Z + N) \cdot [1 - \alpha(q^2)]. \end{aligned} \quad (4)$$

The Γ_{QM} -formulation with $\alpha(q^2)$ provides an intuitive physics understanding and quantitative description on the reduction of νA_{el} cross-sections in terms of QM phase-angle alignment and coherency. In particular, it naturally leads to the limiting behavior at the complete coherency ($\alpha=1$ at $q^2 \sim 0$) and decoherency ($\alpha=0$ at $q^2 \gtrsim [\pi/R]^2$) states, corresponding to $(d\sigma/dq^2) \propto [\varepsilon Z - N]^2$

TABLE I: Summary of the three formulations which characterize the many-body physics in νA_{el} , and the values of the key parameters at the limiting domains where the scattering amplitudes are either completely in phase (“Coherency”) or decoupled (“Decoherency”).

Conditions	Complete Coherency	Complete Decoherency
q^2	$\rightarrow 0$	$\gtrsim \left[\frac{\pi}{R}\right]^2$ with A -Dependence
(I) $\Gamma_{NP}(q^2) = [\varepsilon Z F_Z(q^2) - N F_N(q^2)]^2$		
$F_Z(q^2)$	1	—
$F_N(q^2)$	1	—
$\Gamma_{NP}(q^2)$	$(\varepsilon Z - N)^2$	$(\varepsilon^2 Z + N)$
(II) $\Gamma_{QM}(q^2) = (\varepsilon Z - N)^2 \alpha(q^2) + (\varepsilon^2 Z + N) [1 - \alpha(q^2)]$		
$\phi(q^2)$	0	$\pi/2$
$\alpha(q^2)$	1	0
(III) $\Gamma_{DATA}(q^2) = (\varepsilon Z - N)^2 \xi(q^2)$		
$\xi(q^2)$	1	$\left[\frac{(\varepsilon^2 Z + N)}{(\varepsilon Z - N)^2}\right]$
$\left[\frac{d\sigma}{dq^2}\right](q^2)$	$\propto (\varepsilon Z - N)^2$	$\propto (\varepsilon^2 Z + N)$

and $(d\sigma/dq^2) \propto [\varepsilon^2 Z + N]$, respectively. The experimentally measured $\alpha(q^2)$ -values from different isotope targets can be directly compared to reveal their varying degrees of coherency in the respective processes.

An alternative measurement-driven description, denoted by $\xi(q^2)$, is the cross-section reduction relative to that of complete coherency condition [6], where

$$\Gamma(q^2) \equiv \Gamma_{DATA}(q^2) = (\varepsilon Z - N)^2 \cdot \xi(q^2) \quad . \quad (5)$$

The functions Γ_{NP} , Γ_{QM} and Γ_{DATA} are complementary descriptions of the νA_{el} interactions. The experimentally measurable cross-section reduction fraction (ξ in Γ_{DATA}) is related to QM coherency (α in Γ_{QM}) and nuclear form factors via, respectively,

$$\xi(q^2) = \alpha(q^2) + [1 - \alpha(q^2)] \left[\frac{(\varepsilon^2 Z + N)}{(\varepsilon Z - N)^2} \right] \quad (6)$$

and

$$\xi(q^2) = \frac{[\varepsilon Z F_Z(q^2) - N F_N(q^2)]^2}{(\varepsilon Z - N)^2} \quad , \quad (7)$$

while the two physics descriptions are connected by:

$$[\varepsilon Z F_Z(q^2) - N F_N(q^2)]^2 = (\varepsilon Z - N)^2 \cdot \alpha(q^2) + (\varepsilon^2 Z + N) \cdot [1 - \alpha(q^2)] \quad . \quad (8)$$

The relations between ξ and Γ_{NP} with α for three representative nuclei are shown in Figures 1a&b, respectively. Contours of maximum- q^2 for different neutrino sources are marked in Figure 1b. The behavior

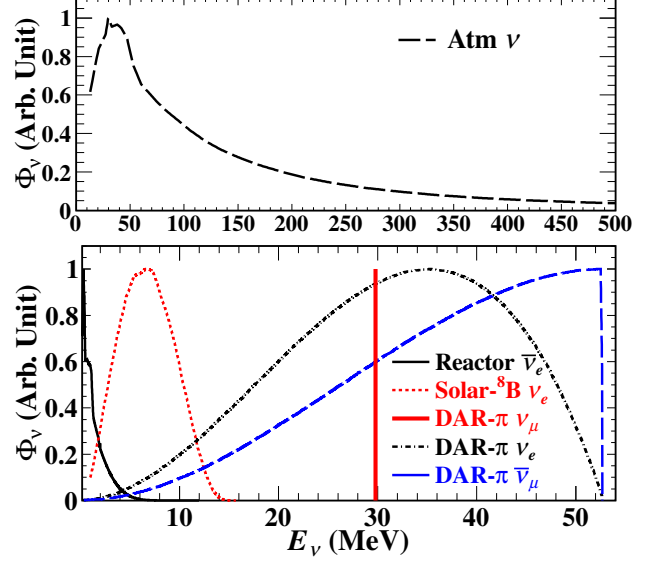


FIG. 2: Neutrino spectra (Φ_ν) from (top) atmospheric as well as (bottom) reactor $\bar{\nu}_e$, solar $^8\text{B } \nu_e$ and DAR- π (ν_μ , ν_e , $\bar{\nu}_\mu$) neutrinos adopted from Refs. [15, 21] and normalized by their maxima.

of Γ_{NP} , α and ξ at the limiting domains corresponding to the complete coherency and decoherency conditions are summarized in Table I. In particular, the relation $\Gamma_{NP} = (\varepsilon^2 Z + N)$ for completely decoherent νA_{el} interactions is a result that emerges by relating Γ_{NP} and Γ_{QM} in Eq. 8, and could not be derived by considerations of nuclear form factor of Eq. 3 alone.

III. PROJECTED EXPERIMENTAL RANGES

The functions Γ_{NP} , Γ_{QM} and Γ_{DATA} can be directly measured from νA_{el} data without input from the underlying physics. Prior to actual measurements, specific formulations of the nuclear form factors have to be adopted for phenomenological studies and to establish the typical ranges to guide the choices of experimental parameters. To serve these purposes, the frequently adopted approach is to take the nuclear form factors for protons and neutrons are identical: $F_N(q^2) = F_Z(q^2) \equiv F_A(q^2)$, and to use the effective “Helm Form Factor” description of Ref. [20]:

$$F_A(q^2) = \left[\frac{3}{qR_0} \right] j_1(qR_0) \exp \left[-\frac{1}{2} q^2 s^2 \right] \quad , \quad (9)$$

where $j_1(x) = [(\sin x/x^2) - (\cos x/x)]$ is the first-order spherical Bessel function. The nuclear dependence appears through $R_0^2 = R^2 - 5s^2$, where $s = 0.5$ fm is the surface thickness of the nuclei. In this formulation, the squared-form factor is equivalent to the cross-section reduction fraction: $[F_A(q^2)]^2 = \xi(q^2)$.

Typical spectra of reactor, solar and atmospheric neutrinos [21], as well as those due to decay-at-rest π

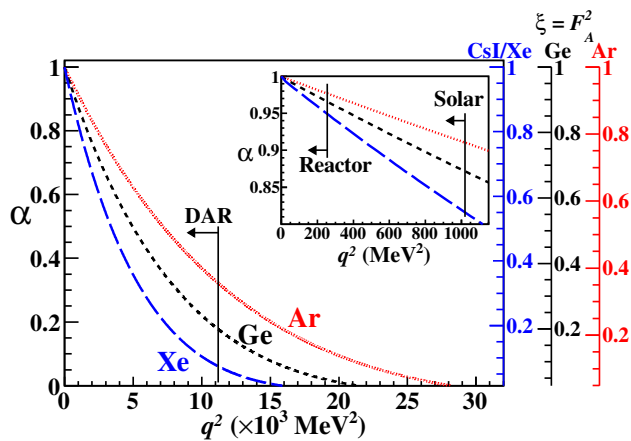


FIG. 3: The variation of α and $\xi (= F_A^2)$ as a function of q^2 of νA_{el} on the three selected nuclei. Different neutrino sources share the same contour for the same target in q^2 -space, but with different ranges. The end-points for reactor, solar and DAR- π neutrinos are marked.

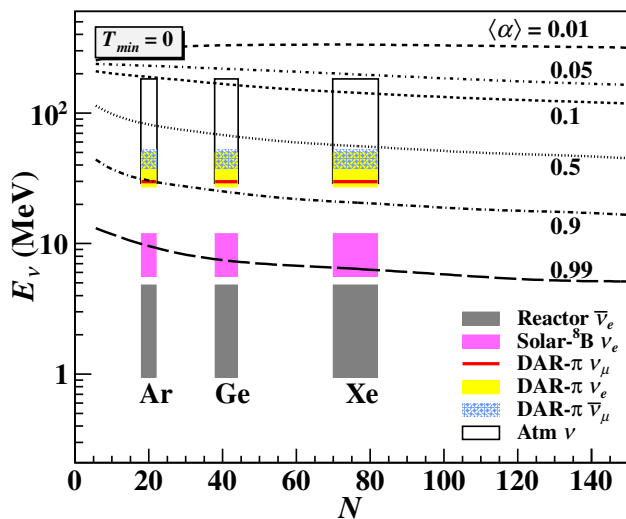


FIG. 4: The contours of the mean degree of coherency $\langle \alpha \rangle$ on the (N, E_ν) plane at $T_{min}=0$, with bands of neutrino sources and target nuclei superimposed. The ranges in E_ν correspond to FWHM in $[\Phi_\nu \cdot \sigma_{\nu A_{el}}]$.

(DAR- π) [15], are used in this study. These are depicted in Figure 2.

The measurable total cross-section is given by convoluting Eq. 2 with the neutrino spectrum $\Phi_\nu(E_\nu)$, and integrating over E_ν and $q^2 \in [q_{min}^2, q_{max}^2]$, from which the mean reduction fraction $\langle \xi \rangle$ and the mean coherency factor $\langle \alpha \rangle$ can be derived [19].

The νA_{el} processes on several nuclei of experimental interest and at different mass ranges are studied – (Ar;Ge;Xe) with $Z=(18;32;54)$. The target that provides the first νA_{el} measurements [15] – CsI, having $Z=55$ and 53, respectively, can be approximated as Xe in this discussion.

The variations of α and $\xi (= F_A^2)$ with q^2 of the four neu-

trino sources, with three selected nuclei (Ar;Ge;Xe) are depicted in Figure 3. The q^2 -dependence is universal for the different neutrino sources, though their q_{max}^2 -values are distinct due to their varying maximum E_ν . These spectra end-points for reactor, solar and DAR- π neutrinos are well-defined, and their corresponding ranges in α and q^2 are depicted in Figures 1b&3, respectively.

A summary plot on the variations of $\langle \alpha \rangle$ with the neutrino sources and target nuclei is illustrated in Figure 4, in which the ranges in E_ν are defined by the Full-Width-Half-Maximum (FWHM) of $[\Phi_\nu \cdot \sigma_{\nu A_{el}}]$. For completeness, the differential and integral event rates due to the four neutrino sources in measurable nuclear recoil energy T , together with their corresponding α and $\langle \alpha \rangle$ values, are discussed and presented in Appendix A.

It can be seen that coherency is mostly complete ($\alpha > 95\%$) for νA_{el} with reactor and solar neutrinos, whereas coherency is only partial for DAR- π and weak for atmospheric neutrinos. Accordingly, studies of νA_{el} with different neutrino sources provide complementary information and cover the transitions from completely coherent to decoherent states.

IV. MEASUREMENTS FROM CURRENT DATA

The COHERENT-CsI(Na) and -Ar experiments at the DAR- π beam with the Spallation Neutron Source facility at the Oak Ridge National Laboratory have provided positive measurements on νA_{el} .

While the first-generation ‘discovery’ measurements cannot be expected to provide severe constraints on $\alpha(q^2)$, it is instructive to go through the data analysis to establish the ranges of the effects and to check consistency.

The published event rates and statistical uncertainties from the COHERENT CsI(Na) [15] and Ar [16] data were adopted as input in this analysis. What were measured per event are the numbers of photo-electrons. To convert these to nuclear recoil energy for physics interpretation, the knowledge of quenching factor (QF) is necessary. The Ar results of Ref. [16] has QF incorporated already. The uncertainties of the QF-model used to derive the first results of CsI(Na) in Ref. [15] were at $\sim 25\%$. For this analysis, a subsequent improved QF-measurement by the same Collaboration [22] were adopted, in which an accuracy of $\sim 3.6\%$ was stated. We note that a previous independent QF-measurement [23] provided results consistent with this one at a $\sim 14\%$ level.

Folding in published signal efficiencies, the efficiency-corrected event rates in different q^2 -bins were derived and are depicted in Figures 5a&b for CsI and Ar, respectively. These were compared with the complete coherency conditions in which $\alpha=1$ ($\phi=0$) and equivalently $\Gamma(q^2)=(\epsilon Z - N)^2$ is set in Eq 2. Expected spectra for the completely decoherent cases are also displayed.

The systematic uncertainties of this analysis were taken from the published estimates discarding the com-

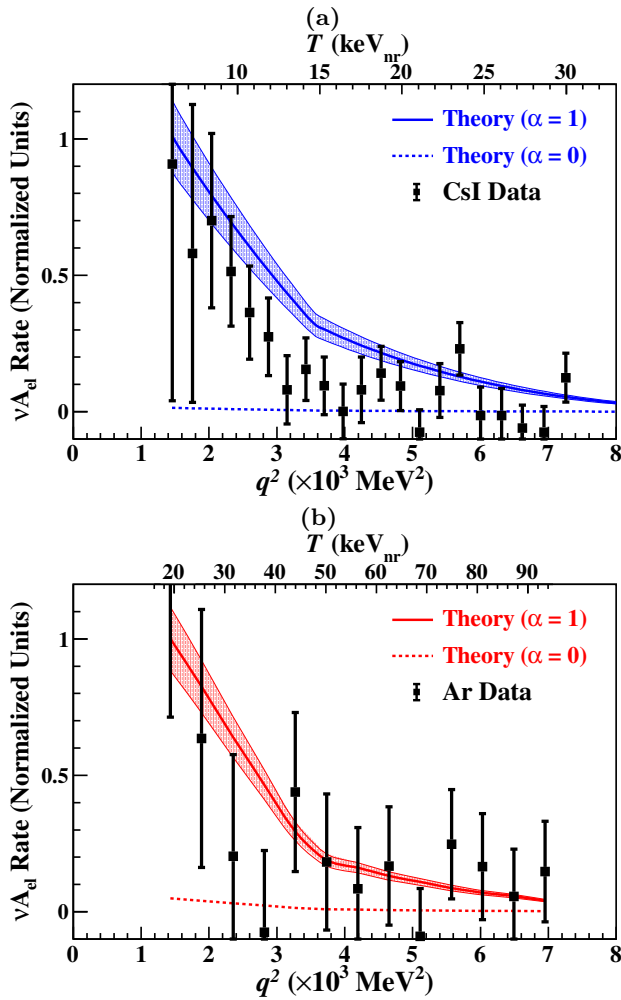


FIG. 5: Efficiency-corrected differential event rates with their statistical uncertainties derived from the COHERENT (a) CsI(Na) [15, 22] and (b) Ar [16] data. Superimposed are the predicted theory bands at the complete coherency ($\alpha=1$) condition, where $\Gamma(q^2)=(\epsilon Z-N)^2$ is set in Eq. 2. Systematic uncertainties are represented by the width of the bands. Their ratios give rise to the cross-section reduction ratios ξ , from which $\alpha(q^2)$ is derived via Eq. 6. The allowed intervals and p-values follows from standard Gaussian statistics [24]. The maxima of the Theory bands within the analyzed ranges are normalized to unity. The complete decoherency conditions ($\alpha=0$) are denoted by dotted lines.

ponent due to nuclear form factors. This corresponds to 11.7% [15, 22] and 11.6% [16] for CsI and Ar, respectively. These are represented by the width of the complete coherency bands in Figures 5a&b. Systematic uncertainties are correlated in q^2 in general. In practice, statistical accuracies dominate the uncertainties at the current level of sensitivities, as shown by comparing the theory band width with the data error bars in Figures 5a&b. Accordingly, the systematic errors are *assumed* to be uncorrelated in q^2 . They are combined bin-wise in quadrature with the statistical errors to produce the total uncertainties. Under this error estimation scheme, the systematic

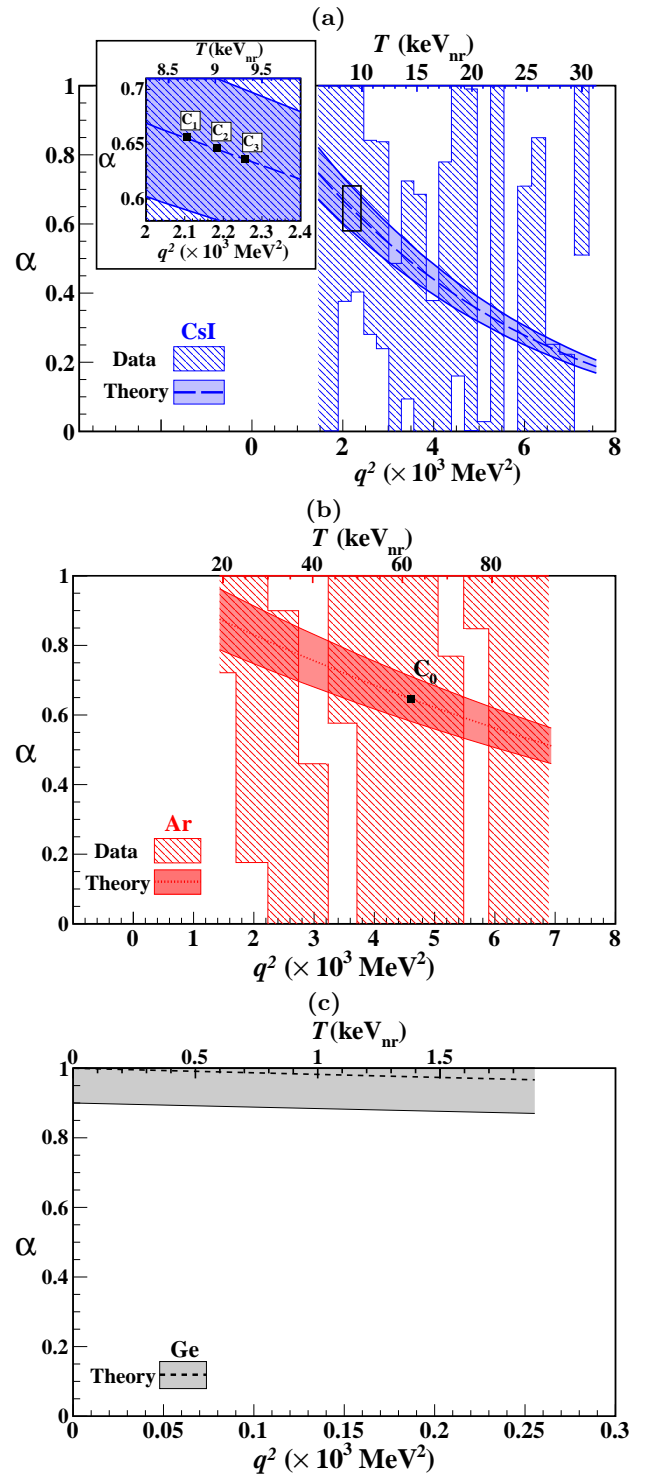


FIG. 6: Measurements on α from COHERENT (a) CsI [15, 22] and (b) Ar [16] data with DAR- π - ν . The stripe-shaded areas are the $1\text{-}\sigma$ allowed regions derived from the reduction in cross-section relative to the complete coherency conditions independent of nuclear physics input. The dark-shaded regions are the theoretical expectations adopting the nuclear form factor formulation of Eq. 9 with a $\pm 1\sigma$ uncertainty of 10%. The $\alpha(q^2)$ -values for different nuclei can be consistently compared. Labels $C_{0,1,2,3}$ correspond to the configurations in Figure 1a where $\alpha_0 < \alpha_1$, $\alpha_0 = \alpha_2$ and $\alpha_0 > \alpha_3$ despite having $\xi_0 > \xi_{1,2,3}$ in all cases. (c) The sensitivity with the theoretical projections applied to reactor- ν on Ge covering the complete q^2 -range for nuclear recoils.

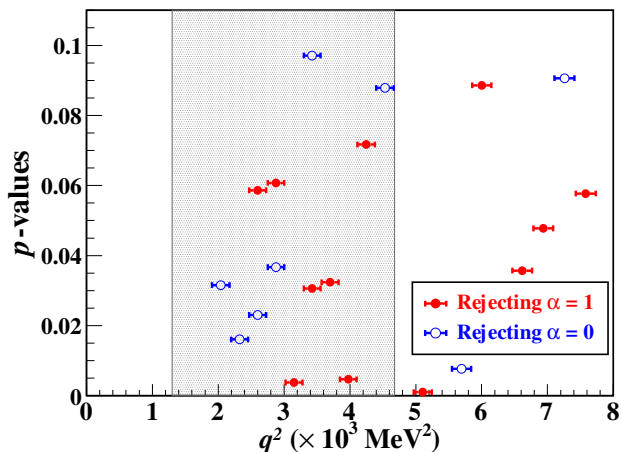


FIG. 7: The p -value significance to probe the specific cases corresponding to the complete coherency ($\alpha=1$ and $\phi=0$, in red) and decoherency ($\alpha=0$ and $\phi=\pi/2$, in blue) conditions from the COHERENT-CsI data [15, 22]. The shaded band corresponds to the stated region-of-interest in Ref. [15] where physics analysis was performed.

effects contribute to $<4\%$ and $<1.5\%$ of the total uncertainties over all q^2 -bins for CsI and Ar, respectively.

The cross-section reduction fractions $\xi(q^2)$ were evaluated, from which $\alpha(q^2)$ and their uncertainties were extracted using Eq. 6. The various measures which characterize allowed and excluded intervals at each q^2 -bin were then derived with the standard statistics procedures [24], assuming Gaussian errors.

The allowed $1-\sigma$ ranges in $\alpha(q^2)$ are depicted as stripe-shaded regions in Figures 6a&b for CsI and Ar, respectively. These results are data-driven without invoking nuclear physics input. Measurements and implications of every q^2 -bin are independent of and uncorrelated with the others, and therefore the allowed intervals in adjacent bins are discontinuous.

The different q^2 -bins become correlated when the nuclear form factors of Eq. 9 are adopted and imposed as theoretical expectations. The predicted parameter space from measurements with projected 10% uncertainty at $\pm 1\sigma$ -level is superimposed as dark-shaded bands, showing the cases with CsI (equivalently, Xe) and Ar at DAR- π . The projected sensitivity for reactor- ν on Ge is displayed in Figure 6c, showing that measurements with reactor νA_{el} can probe the complete coherency regime. A bin-wise 10% uncertainty corresponds to an appropriate sensitivity target for future experiments. It is the scale where systematic effects start to contribute, and the measurements can make strong tests on the extreme cases of $\alpha=0(1)$ as well as making comparisons with nuclear form factor predictions.

It can be seen that the current data are consistent with the predictions from Eq. 9. Future measurements with sufficient accuracies would probe the transitions in QM

coherency according to:

$$\begin{aligned}
 &\text{CsI/Xe @ DAR-}\pi : \\
 &\quad \alpha \in [0.72, 0.14] \text{ for } T \in [6.6, 36] \text{ keV}_{\text{nr}} \\
 &\text{Ar @ DAR-}\pi : \\
 &\quad \alpha \in [0.88, 0.51] \text{ for } T \in [19, 93] \text{ keV}_{\text{nr}} \\
 &\text{Ge @ Reactor(Projected) :} \\
 &\quad \alpha \in [1.00, 0.96] \text{ for } T \in [0, 1.9] \text{ keV}_{\text{nr}} ,
 \end{aligned} \tag{10}$$

following the T -ranges used in Figure 6.

The significance in terms of p -values [24] for testing the specific cases of $\alpha=1(0)$, equivalently $\phi=0(\pi/2)$, with the CsI data are depicted in Figures 7. In particular, the most stringent bounds within the stated region-of-interest in Ref. [15] in excluding complete QM coherency and decoherency at 90% confidence levels with specified p -values are, respectively,

$$\begin{aligned}
 &\alpha < 0.57 \\
 &\phi < 0.61 \cdot (\pi/2) \\
 &p = 0.004
 \end{aligned} \tag{11}$$

at $q^2=3.1 \times 10^3 \text{ MeV}^2$ and

$$\begin{aligned}
 &\alpha > 0.30 \\
 &\phi > 0.80 \cdot (\pi/2) \\
 &p = 0.016
 \end{aligned} \tag{12}$$

at $q^2=2.3 \times 10^3 \text{ MeV}^2$. These results verify that both QM superpositions among the nucleonic scattering centers and nuclear many-body effects contribute to the νA_{el} process.

These diverse ranges of α -sensitivity indicate the complementarity of νA_{el} measurements among reactor and DAR- π neutrinos. Future measurements of solar νA_{el} [14] with multi-ton detectors would probe a similar range of α as reactor neutrinos. Xenon detectors with scale $\mathcal{O}(100)$ ton would be required to probe the weakly-coherent region at $\alpha < 0.2$ with atmospheric neutrinos.

V. SUMMARY AND PROSPECTS

Neutrino-nucleus elastic scattering – the interaction νA_{el} in Eq. 1 – involves two distinct concepts: elastic kinematics and QM-coherency. It provides a laboratory to study QM-superpositions in electroweak interactions. The QM-coherency aspect should be characterized by distributions with dependence on $A(Z, N)$ and q^2 . Descriptions of coherency as a binary state or having both concepts bundled together may have the unintended consequences of missing the complexities of the process and suppressing the potential richness of its physics content. We formulated a quantitative and universal parametrization of the QM-coherency [6] to facilitate studies of QM-effects in νA_{el} , under which the fundamental parameter is the experimentally accessible misalignment phase-angle

TABLE II: Averaged $[\langle\alpha\rangle; \langle\xi\rangle]$ and total event rates in $\text{kg}^{-1}\text{day}^{-1}$ for the target nuclei at a threshold of 1 and 10 keV_{nr} and for different ν -sources. Reactor and DAR- π neutrino fluxes are taken to be $10^{13} \text{ cm}^{-2}\text{s}^{-1}$, while DAR- π neutrino flux is $3.4 \times 10^{14} \text{ cm}^{-2}\text{yr}^{-1}$ /flavor at 19.3 m from target at beam intensity $2 \times 10^{23} \text{ POT yr}^{-1}$. Rates due to atmospheric neutrinos are from the integration of q^2 -ranges corresponding to $\alpha \in [0.01, 1.0]$.

Detector Target	ν -Sources			
	DAR- π	Reactor	Solar	Atmospheric
	$[\langle\alpha\rangle; \langle\xi\rangle]$		$[\langle\alpha\rangle; \langle\xi\rangle]$	
	Total Event Rates ($\text{kg}^{-1}\text{yr}^{-1}$)		Total Event Rates ($\text{ton}^{-1}\text{yr}^{-1}$)	
	Detector Threshold = 1 keV_{nr}			
Ar	[0.92 ; 0.93] 27.2	[0.99 ; 0.99] 766	[0.98 ; 0.98] 130	[0.61 ; 0.63] 0.019
Ge	[0.84 ; 0.84] 46.1	[0.98 ; 0.98] 138	[0.97 ; 0.97] 140	[0.46 ; 0.47] 0.028
Xe	[0.72 ; 0.72] 77.8	[0.95 ; 0.95] 0.07	[0.94 ; 0.94] 95.7	[0.41 ; 0.42] 0.039
	Detector Threshold = 10 keV_{nr}			
Ar	[0.87 ; 0.87] 19.2	N/A	N/A	[0.57 ; 0.59] 0.017
Ge	[0.72 ; 0.72] 22.6	N/A	N/A	[0.37 ; 0.39] 0.022
Xe	[0.46 ; 0.47] 17.1	N/A	N/A	[0.24 ; 0.25] 0.021

(ϕ , equivalently as $\alpha \equiv \cos\phi$) between non-identical nucleonic scattering centers.

Current positive measurements on νA_{el} provide only weak constraints to $\alpha(q^2)$ and equivalently misalignment phase-angle $\phi(q^2)$. Data with $\mathcal{O}(10\%)$ accuracy would allow the studies of transitions in QM-coherency over a wide range in $\alpha \in [0, 1]$.

The νA_{el} process described in terms of QM-effects (Γ_{QM}) is complementary to the conventional descriptions with nuclear form factors (Γ_{NP}) based on the many-body physics in the nucleon-nucleus interplay. Both formulations are related with the directly measurable cross-section reduction fraction (ξ), and among themselves, via Eqs. 6,7&8.

The α -parameter quantifies QM-coherency in νA_{el} and adds preciseness to the qualitative discussions. While the *derivation* of the α -values depends on $A(Z, N)$ and q^2 in similar footing as those for Γ_{NP} , the *interpretation* of measurements with α in terms of degrees of QM-coherency or scattering phase-angle alignment is universal among different configurations with varying nuclei and q^2 . This feature allows the quantitative characterization of the configurations and is not available with the ξ or Γ_{NP} frameworks. Referring to an example illustrated in Figure 1a, the four cases $C_{0,1,2,3}$ are all within the DAR- π measurable kinematics domain. It can be inferred that Configuration- C_0 with Ar has the same QM-coherency as C_2 in CsI ($\alpha_0 = \alpha_2$) while having lower and higher levels of coherency than C_1 ($\alpha_0 < \alpha_1$) and C_3 ($\alpha_0 > \alpha_3$), respectively, despite the nuclear targets and interaction kinematics (q^2 and T) are different and the

cross-section reduction $\xi_0 > \xi_{1,2,3}$ apply in all cases.

New measurements on νA_{el} from a variety of neutrino sources and nuclear targets can be expected. To facilitate comprehensive book-keeping of the expanding array of data from diverse configurations, it would be beneficial to include the α -parameter as a qualifier on QM-coherency to each measurement, in the similar spirit as adopting q^2 to qualify the interaction kinematics.

The quantitative description of QM-superpositions with the α -parameter among the scattering amplitudes between individual nucleons may serve as natural entry-points to some BSM studies, such as those where both coherent and decoherent channels would contribute to νA_{el} [25]. The experimentally measurable relation between Γ_{NP} and α in Figure 1b describes the transitions in QM-coherency in terms of the evolution from nuclear to nucleon effects in νA_{el} interaction. Understanding and applications of these are possible topics of future research, but are beyond the scope of the present work.

VI. ACKNOWLEDGEMENT

This work is supported by the Academia Sinica Principal Investigator Award AS-IA-106-M02, Contracts 106-2923-M-001-006-MY5, 107-2119-M-001-028-MY3 and 109-2112-M-259-001 from the Ministry of Science and Technology, Taiwan, and 2017-ECP2 from the National Center of Theoretical Sciences, Taiwan. We are grateful to the Reviewer for bringing to our attention new quenching factor measurements of Ref. [22] after the

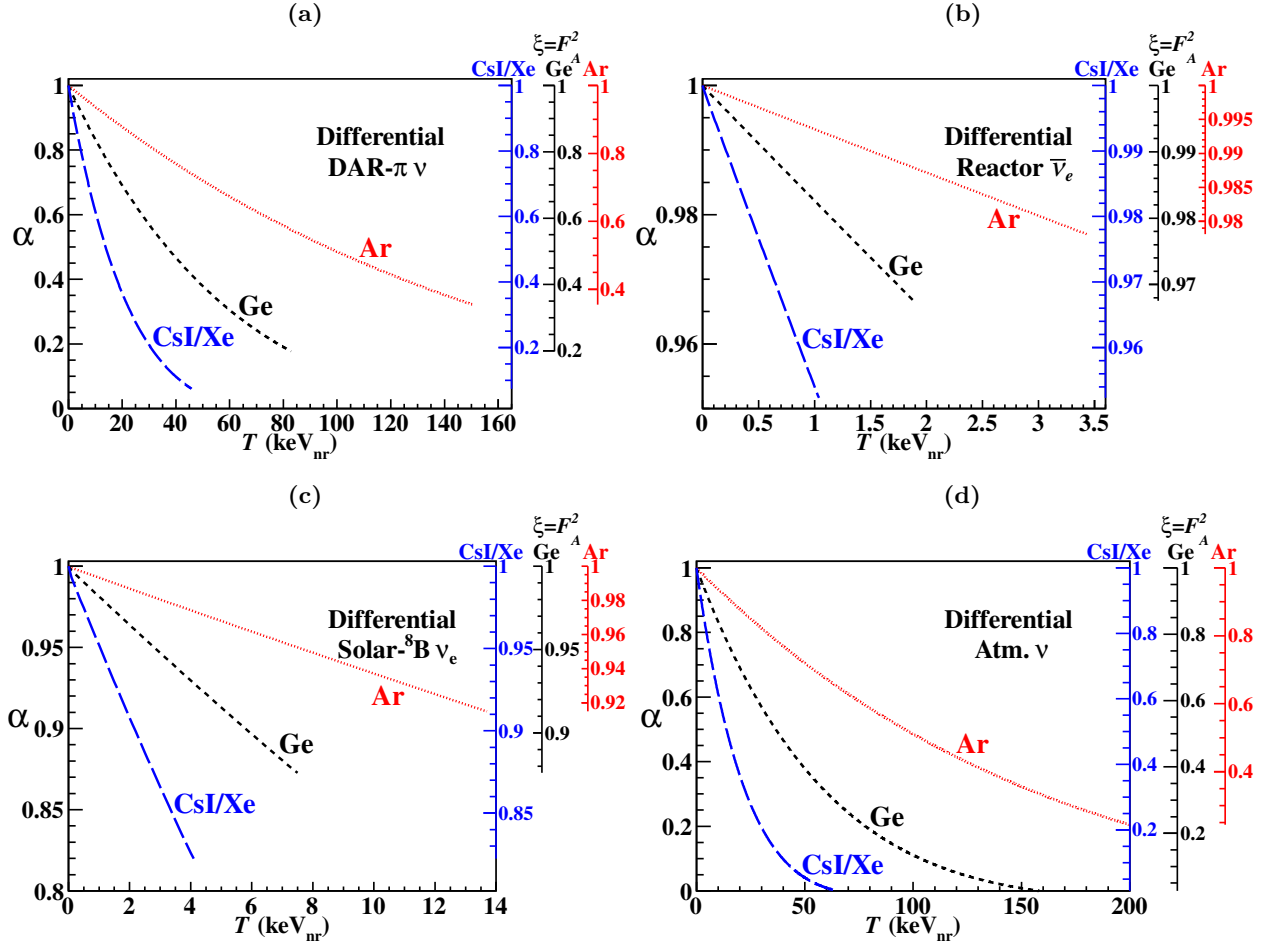


FIG. 8: The variations of α and $\xi(=F_A^2)$ with T in νA_{el} on the three selected nuclei for (a) DAR- π , (b) Reactor, (c) Solar, and (d) Atmospheric neutrinos.

initial completion of this work. This article is dedicated to the memory of Dr. Saime Kerman.

Appendix A: Measurable Event Rates

The differential cross-section of Eq. 2 on q^2 can be translated to one as function of the measurable nuclear recoil-energy T by

$$\left[\frac{d\sigma}{dT} \right]_{\nu A_{el}} = 2M \left[\frac{d\sigma}{dq^2} \right]_{\nu A_{el}}. \quad (\text{A1})$$

The differential spectra (dR/dT) convoluted with the neutrino spectrum $\Phi_\nu(E_\nu)$ is given by:

$$\left(\frac{dR}{dT} \right)_{\nu A_{el}} = 2M \int \left[\left(\frac{d\sigma}{dq^2} \right)_{\nu A_{el}}(T, E_\nu) \right] \Phi_\nu(E_\nu) dE_\nu. \quad (\text{A2})$$

Integration over $T \in [T_{min}, T_{max}]$ gives the total event rates.

The universality of Figure 3 no longer applies when q^2 is replaced by T . The variations of α , F_A and ξ with T depend on E_ν -distributions and therefore neutrino sources. The variations are depicted in Figure 8.

The differential rates derived from the four sources and three targets are displayed in Figure 9. The corresponding total rates are shown in Figure 10, showing their variations with T_{min} and $\langle \alpha \rangle$. The values of $\langle \alpha \rangle$ and $\langle \xi \rangle$ as well as the total event rates at $T_{min}=1(10)$ keV_{nr} for the various neutrino sources and target nuclei are summarized in Table II. Evaluation of these rates are based on standard solar and atmospheric spectra [21]. Reactor $\bar{\nu}_e$ flux is taken to be 10^{13} cm⁻²s⁻¹, while DAR- π per-flavor neutrino flux is 3.4×10^{14} cm⁻²yr⁻¹ corresponding to 2×10^{23} proton-on-target(POT)/year at 19.3 m from target [15]. There is no high-energy cut-off in E_ν for the atmospheric neutrino spectra. The differential and integral spectra of Figures 9&10d are therefore evaluated for $\alpha \in [0.01, 1.0]$, corresponding to $T < (361; 148; 60)$ keV_{nr} for (Ar; Ge; Xe).

Typically, measurements of νA_{el} with reactor and solar neutrinos require $\mathcal{O}(1)$ keV_{nr} detector threshold giving expected rates of $\mathcal{O}(1)$ /kg-day and $\mathcal{O}(1)$ /ton-yr, respec-

tively. The corresponding event rates for DAR- π and atmospheric neutrinos are $\mathcal{O}(10)/\text{kg}\cdot\text{yr}$ and $\mathcal{O}(0.01)/\text{ton}\cdot\text{yr}$ at a threshold of $\mathcal{O}(10)\text{keV}_{\text{nr}}$, respectively.

At the detection threshold of 1 keV_{nr} , 90% of the elastic scattering events between Weakly Interacting Massive Particles (WIMPs)-dark matter of mass 1 TeV with (Ar;Ge;Xe)-target have recoil energy up to

$(99;74;35)\text{ keV}_{\text{nr}}$. These kinematics ranges correspond to α as low as $(0.49;0.22;0.14)$ for νA_{el} scattering with atmospheric neutrinos, as indicated in Figure 8d – far from the complete coherency regime. Accordingly, the description of “the neutrino floor originates from *coherent* neutrino-nucleus scattering” is not applicable for WIMPs at TeV or higher mass scales.

-
- [1] D.Z. Freedman, Phys. Rev. **D 9**, 1389 (1974); D.Z. Freedman, D.N. Schramm, and D.L. Tubbs, Ann. Rev. Nil. Part. Sci. **27**, 167 (1977).
- [2] D.K. Papoulias and T.S. Kosmas, Adv. High Energy Phys. **2015**, 763648 (2015).
- [3] L.M. Krauss, Phys. Lett. **B 269**, 407 (1991); J. Barranco, O.G. Miranda and T.I. Rashba, JHEP. **12**, 021 (2005); J. Barranco, O.G. Miranda and T.I. Rashba, Phys. Rev. **D 76**, 073008 (2007); D.K. Papoulias et al., Phys. Rev. **D 102**, 113004 (2020).
- [4] K. Scholberg, Phys. Rev. **D 73**, 033005 (2006).
- [5] J.R. Wilson, Phys. Rev. Lett. **32**, 849 (1974).
- [6] S. Kerman et al., Phys. Rev. **D 93**, 113006 (2016).
- [7] K. Patton et al., Phys. Rev. **C 86**, 024612 (2012); E. Ciuffoli et al., Phys. Rev. **D 97**, 113003 (2018); M. Cadeddu et al., Phys. Rev. Lett. **120**, 072501 (2018); D.A. Sierra et al., J. High Energy Phys. **2019**, 141 (2019); C.G. Payne, Phys. Rev. **C 100**, 061304(R) (2019); P. Coloma et al., J. High Energy Phys. **08**, 030 (2020).
- [8] C.J. Horowitz, K.J. Coakley, and D.N. McKinsey, Phys. Rev. **D 68**, 023005 (2003).
- [9] J. Learned, Nucl. Phys. B (Proc. Suppl.) **143**, 152 (2005).
- [10] J. Monroe and P. Fisher, Phys. Rev. **D 76**, 033007 (2007); A. Gütlein et al., Astropart. Phys. **34**, 90 (2010); J. Billard, E. Figueroa-Feliciano, and L. Strigari. Phys. Rev. **D 89**, 023524 (2014).
- [11] M. Drees and G. Gerbier, Review of Particle Physics, Phys. Rev. **D 98**, 030001:396 (2018), and references therein.
- [12] H.T. Wong et al., J. Phys. Conf. Ser. **39**, 266 (2006); V. Belov et al., J. Instrum. **10**, P12011 (2015); G.F. Moroni et al., Phys. Rev. **D 91**, 072001 (2015); A.K. Soma et al., Nucl. Instrum. Meth. **A 836**, 67 (2016); G. Agnolet et al., Nucl. Instrum. Meth. **A 853**, 53 (2017); C. Buck et al., J. Phys. Conf. Ser. 1324.012094 (2020); J. Roth et al., J. Low Temp. Phys. **199**, 433 (2020).
- [13] F.T. Avignone and Yu.V. Efremenko, J. Phys. **G 29**, 2615 (2003); D. Akimov et al., arXiv:1509.08702 (2015) and references therein for current experimental projects.
- [14] L.E. Strigari et al., New J. Phys. **11**, 105011 (2009); L. Baudis et al., J. Cos. Astropart. Phys. **01**, 044 (2014).
- [15] J.I. Collar et al., Nucl. Instrum. Meth. **A 773**, 56 (2015); D. Akimov et al., Science **357**, 1123 (2017), and Supplementary Materials.
- [16] D. Akimov et al., Phys. Rev. **D 100**, 115020 (2019); D. Akimov et al., Phys. Rev. Lett. **126**, 012002 (2021), and Supplementary Materials.
- [17] I. Angeli and K.P. Marinova, At. Data Nucl. Data Tables **99**, 69 (2013); J.E. Amaro et al., arXiv 1912.1061 (2019).
- [18] T.W. Donnelly, J. Dubach, and I. Sick, Nucl. Phys. **A 503**, 589 (1989).
- [19] The α and ξ results of Ref. [6] are mean values equivalent to $\langle\alpha\rangle$ and $\langle\xi\rangle$, respectively, in this article.
- [20] J. Engel, Phys. Lett. **B 264**, 114 (1991).
- [21] J.N. Bahcall et al., Phys. Rev. Lett. **92**, 121301 (2004); G. Battistoni et al., Astropart. Phys. **23**, 526 (2005); H.T. Wong et al., Phys. Rev. **D 75**, 012001 (2007).
- [22] A. Konovalov, in *Magnificent CE ν NS* (2020), <https://indico.cern.ch/event/943069/contributions/4066385/>.
- [23] J.I. Collar et al., Phys. Rev. **D 100**, 033003 (2019).
- [24] G. Cowan, Review of Particle Physics, Phys. Rev. **D 98**, 030001:527, Section 39.4.2.2, (2018).
- [25] M. Hoferichter, J. Menendez and A. Schwenk, Phys. Rev. **D 102**, 074018 (2020).

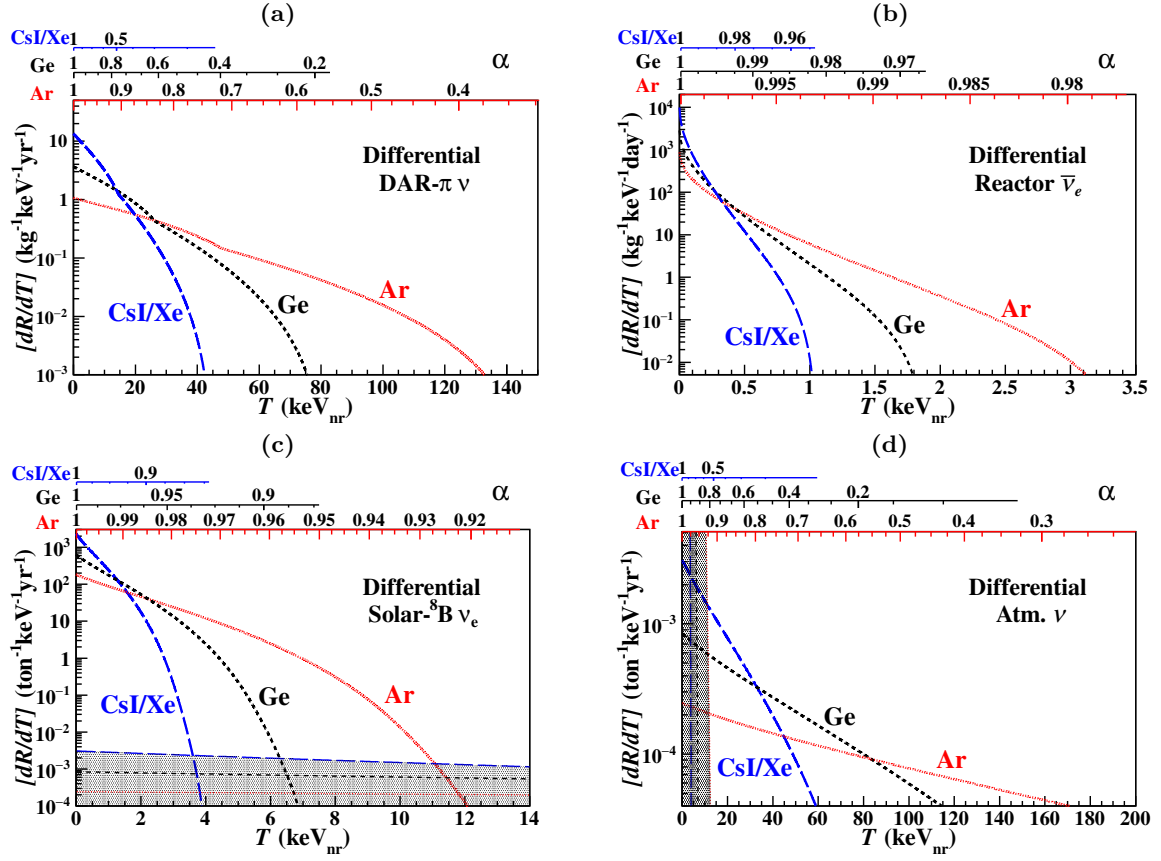


FIG. 9: Differential event rates $[dR/dT]$ of νA_{el} on the three selected nuclei, and their correlations with α , with (a) DAR- π , (b) Reactor, (c) Solar, and (d) Atmospheric neutrinos. Superimposed as shaded regions in (c) and (d) are the background rates due to atmospheric and solar neutrinos, respectively.

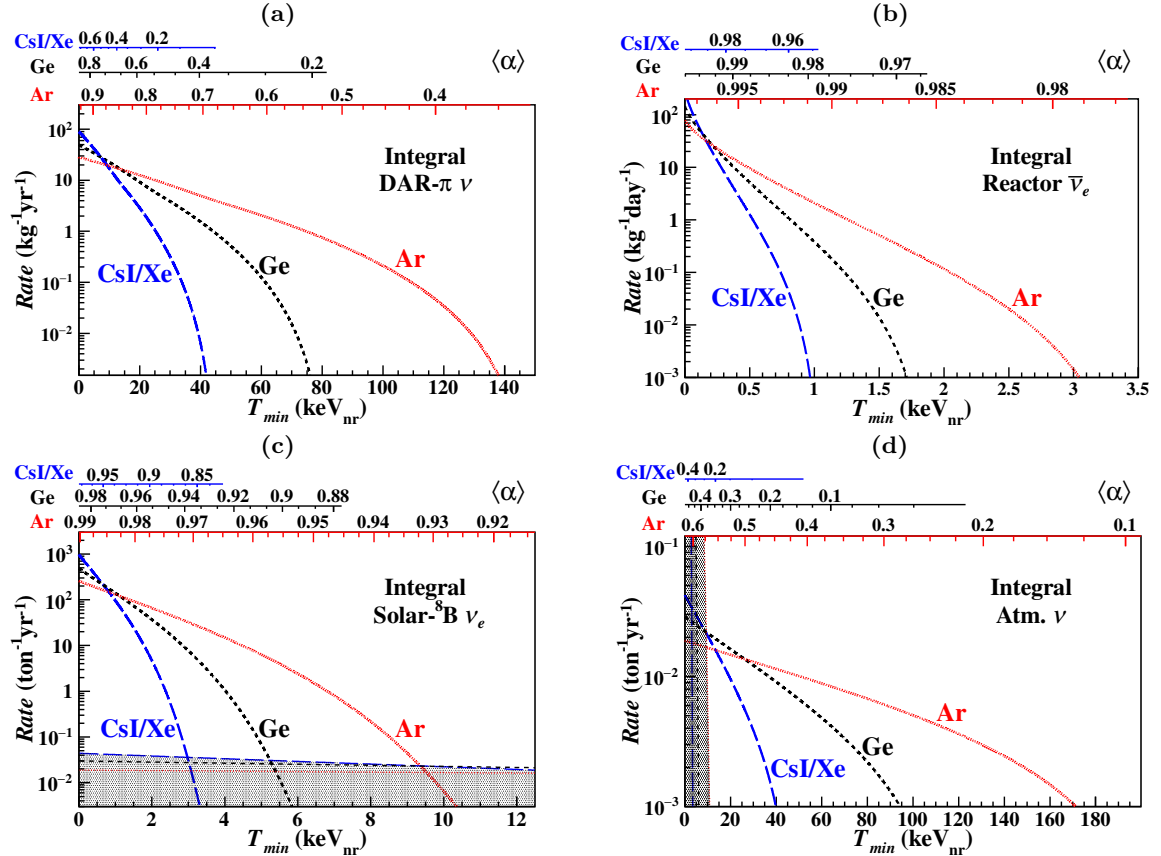


FIG. 10: Integral event rates of νA_{el} on the three selected nuclei as functions of threshold T_{min} , and their correlations with $\langle\alpha\rangle$ for (a) DAR- π , (b) Reactor, (c) Solar, and (d) Atmospheric neutrinos. Superimposed as shaded regions in (c) and (d) are the background rates due to atmospheric and solar neutrinos, respectively.